Chemical Engineering Journal 472 (2023) 144894

Contents lists available at ScienceDirect

Chemical Engineering Journal

journal homepage: www.elsevier.com/locate/cej

Trace cisplatin and carboplatin removal by 3-mercaptopropionic acid and L-cysteine functionalized sponges: Adsorption behaviour and mechanism

Dong Han [a], Montserrat López-Mesas [a,*], Roberto Boada [a], Tania Farías [b], Ana R. Lazo Fraga [b], Manuel Valiente [a]

[a] GTS-UAB Research Group, Department of Chemistry, Faculty of Science, Universitat Autònoma de Barcelona, Bellaterra, (Cerdanyola del Vallès), 08193 Barcelona, Spain

[b] Institute of Materials Science and Technology, University of Havana, 10400 Havana, Cuba

ARTICLE INFO

Keywords:
Adsorption
Cisplatin
Carboplatin
Pt-based cytostatics
Thiol-functionalization
XAS

ABSTRACT

This study presents functionalized open-celled cellulose Metalzorb® sponge (Sponge) with 3-mercaptopropionic acid (MPA) and L-Cysteine (Cys), and the resulting MPA@Sponge and Cys@Sponge showed significantly improved removal efficiency towards trace cisplatin and carboplatin against Sponge. MPA@Sponge achieved maximum removal of 88.9 ± 0.5% for cisplatin and 85.2 ± 0.4% for carboplatin, while Cys@Sponge achieved maximum removal of 75 ± 2% and 59 ± 1%. In contrast, Sponge only achieved removal of 29 ± 4% and 4 ± 1%, respectively. It suggests that thiol groups serve as favourable binding sites for Pt complexation. Carboplatin exhibits lower adsorption compared to cisplatin due to its limited hydration. However, the presence of Cl^- in stock and high temperature facilitate the hydration and the formation of active derivatives of carboplatin, thereby enhancing its adsorption. The rapid adsorption processes of cisplatin and carboplatin are well described by the pseudo-second-order kinetic model involving diffusion and chemisorption. The results from adsorption isotherms revealed a monolayer adsorption that aligns with the principles proposed by the Langmuir model. High temperature significantly enhances the adsorption, and the positive enthalpies indicate that the binding of Pt with thiol groups is endothermic process. X-ray absorption spectroscopy measurements at the Pt L_3-edge revealed a similar coordination environment of the adsorbed Pt on both functionalized adsorbents, which can be attributed to the formation of four Pt-S bonds during the adsorption. To assess the validity of the adsorption results under realistic medium conditions, an adsorption study was carried out by using diluted urine spiked with trace platinum cytostatic drugs to simulate hospital wastewater. 90.2 ± 0.3% of cisplatin and 77.0 ± 0.2% of carboplatin was effectively removed by MPA@Sponge from diluted urine.

1. Introduction

Cisplatin and carboplatin, well-known platinum cytostatic drugs (Pt-CDs), are widely utilized in cancer therapy and characterized for possessing genotoxicity, mutagenicity, carcinogenicity, and teratogenicity as they attack not only cancer cells but also healthy cells [1]. The presence of these substances in aquatic environments has been identified as a significant hazard to both humans and aquatic organisms that are exposed to them, thereby posing a serious threat [2,3]. Pharmacokinetic investigations provide substantiation that approximately 10–40% of Pt-CDs administered to patients are excreted via urine, either in their original form or as metabolites [4]. These compounds are ultimately released into the environment through the discharge of hospital or domestic wastewaters (the latter contaminated by ambulatory patients), as has been proved by many researchers over the last two decades, with concentrations varying between ng·L^{-1} to 250 μg·L^{-1} [5]. Furthermore, several investigations have verified the harmful impacts of cisplatin and carboplatin on certain aquatic invertebrates, even at low levels, in both freshwater and marine ecosystems [6–12]. Limited efforts have been taken to investigate the viability of efficient wastewater remediation methods for Pt-CDs, utilizing diverse techniques such as adsorption [13–17], membrane separation [18,19], ozonation [20] and electrolysis [21,22]. Among them, adsorption, a well-established technology, is frequently considered a favorable approach due to its inherent simplicity of operation, low cost, easy scalability, and significant treatment efficiency. In fact, some pioneering studies on the adsorption of Pt-

* Corresponding author.
E-mail address: montserrat.lopez.mesas@uab.cat (M. López-Mesas).

https://doi.org/10.1016/j.cej.2023.144894
Received 9 June 2023; Received in revised form 14 July 2023; Accepted 16 July 2023
Available online 17 July 2023

CDs using various materials have already been conducted. As early as 2005, Lenz et al., evaluated the adsorption of three cancerostatic platinum compounds (concentrations ranging from 4.7 to 145 $\mu g \cdot L^{-1}$) by activated sludge, and after 24 h of incubation time, the removal rates reached 96%, 70% and 74% for cisplatin, carboplatin and oxaliplatin respectively [15]. Ogata et al., prepared calcined gibbsite for the adsorption of cisplatin (initial concentration of 10 $mg \cdot L^{-1}$) and achieved a removal efficiency of about 90% [14]. Biomass-derived materials such as activated carbon, biochar, chitosan, and wood ash were proposed for adsorption of inorganic $PtCl_6^{2-}$ as a model of Pt-CDs (initial concentration of Pt within the range of 1 to 10 $mg \cdot L^{-1}$), with adsorption capacities ranging from 0.23 to 0.97 $mg \cdot g^{-1}$ of Pt at an adsorbent dose of 10 $g \cdot L^{-1}$ [16]. Cryogels were synthesized to adsorb cisplatin (250 to 2000 $mg \cdot L^{-1}$), and the maximum adsorption capacity was discovered to be 150 $mg \cdot g^{-1}$, attributed to the formation of a stable complex between Pt and the carboxyl group on methacrylic acid [13], where similar strategies were previously used to synthesize carriers for cisplatin drug delivery [23,24]. Recently, a study proposed ion-imprinted mesoporous organosilica for adsorption of $PtCl_4^{2-}$ as a model of Pt-CDs and a maximum adsorption capacity of 76.4 $mg \cdot g^{-1}$ was attained [17]. Another recent study reported the synthesis of dithiocarbamate-modified silica for the removal of cisplatin at varying concentrations (ranging from 5 to 150 $mg \cdot L^{-1}$ Pt in NaCl 0.9% w/v). The maximum adsorption capacity of the adsorbent was determined to be 15.6 $mg \cdot g^{-1}$, and removal efficiency of up to 85% was observed at a dose of 10 $g \cdot L^{-1}$ of adsorbent and contact time of 1 h [25].

Upon reviewing the aforementioned studies, it becomes evident that the majority of the adsorption experiments predominantly occurred within the $mg \cdot L^{-1}$ concentration range. The establishment of adsorption systems and the elucidation of adsorption mechanisms were based on concentrations that surpassed those observed in actual environmental scenarios. However, the performance assessment of these approaches in the actual treatment of low-concentration Pt-CDs remains unclear. In view of the trace concentration (less than 1 $mg \cdot L^{-1}$) of Pt-CDs, a notable challenge exists in establishing an efficient and rapid adsorption system, owing to the limited concentration gradient at the interface between the liquid and solid phases. Hence, further research efforts ought to be directed towards developing adsorbents that exhibit high selectivity and strong affinity. To attain this goal, exploring and interpreting the adsorption mechanism assumes critical significance. Additionally, it is imperative to consider the economic and operational convenience aspects, to strike a balance between efficiency and cost-effectiveness.

In our previous study, we conducted a comparative analysis of three commercially available materials, namely 3-(diethylenetriamino)propyl-functionalized silica gel, cysteine-functionalized silica gel, and open-celled cellulose MetalZorb® sponge (Sponge), for their adsorption capabilities towards trace amounts of cisplatin and carboplatin [26]. Our results suggest that the presence of thiol groups as affinity sites offered the potential for complexation of the target Pt species [26]. Moreover, following intravenous administration of Pt-CDs, investigations have demonstrated their interaction with diverse constituents of the blood, like human serum albumin (HSA). HSA, being the predominant protein in human blood, comprises cysteine residues that can interact with administered Pt complexes [27–30]. In addition, according to Hard-Soft Acid-Base (HSAB) theory [31], Pt(II) as a "soft" acid has a high affinity for sulfur donors ("soft" bases) *e.g.* thiols and thioethers. Inspired by these findings, the current study sought to improve the adsorption properties of cheap and commercially available Sponge through functionalization with thiol-containing compounds, as 3-mercaptopropionic acid (MPA) and L-Cysteine (Cys). The resulting materials, namely MPA@Sponge and Cys@Sponge, respectively, were then evaluated for their capacity to remove trace cisplatin and carboplatin from aqueous solutions, and compared to raw Sponge. Moreover, the adsorption mechanisms have been explained by the results obtained from synchrotron X-ray absorption spectroscopy (XAS) technique.

2. Materials and methods

2.1. Reagents and materials

Cisplatin (99%, CAS: 15663–27–1) and carboplatin (99%, CAS: 41575–94–4) were acquired from STREM Chemicals. The compounds were utilized in their as-received form without undergoing any further purification. Stock solutions of cisplatin and carboplatin (Pt 100 $mg \cdot L^{-1}$), were firstly prepared in 0.2 $mol \cdot L^{-1}$ HCl and Milli-Q water respectively and were subsequently diluted to the required concentration. MetalZorb® Sponge (Sponge) was generously provided by Clean-Way Environmental Partners, Inc. (Portland, USA). Acetic anhydride (Ac_2O, $\geq$ 99%), 3-mercaptopropionic acid (MPA, $\geq$ 99%) and L-Cysteine (Cys, 97%) were acquired from Sigma-Aldrich. Throughout the experimental procedure, Milli-Q water with a resistivity of 18.2 $M\Omega \cdot m^{-1}$ was utilized, unless explicitly stated otherwise.

2.2. Preparation of thiol-functionalized sponges

The original Sponge utilized in this study has a cube-shaped structure composed of an open-celled cellulose substrate. The dimensions of the cubes were measured to be 13 ± 2 (L) $\times$ 10 ± 1 (W) $\times$ 7 ± 1 (H) mm on average, with an average weight of 0.20 ± 0.02 g per cube. In order to minimize the usage of expensive and toxic Pt-CDs in the adsorption experiments, sponges were employed in powdered form to reduce scale. The cubes underwent mechanical grinding in a commercial blender using knife milling, followed by sieving to achieve the desired particle size of $\leq$ 0.5 mm. The resulting fine sponge powders were washed once with 1.0 $mol \cdot L^{-1}$ HCl and three times with Milli-Q water. After the washing process, the Sponge powders were dried at 353 K for a duration of 24 h and subsequently stored for further use. As illustrated in Fig. 1, the process of thiol-functionalization of Sponge was carried out through esterification, utilizing a modified version of the procedure described in previous studies [32–35]. In a glass tube with screw cap, 10 mL of MPA (114.8 mmol) or 2.5 g of Cys (20.6 mmol) was mixed with 10 mL of Ac_2O and 50 µL of concentrated sulfuric acid. Ac_2O serves as a reaction medium, simultaneously consuming the water generated during the esterification reaction. When cooled to room temperature, 0.5 g of sponge powder was added, and the mixture was stirred in an oven at 338 K for 4 days. The two products generated, namely MPA@Sponge and Cys@Sponge, were subjected to sequential washing with acetone, alcohol, and Milli-Q water, and subsequently dried at 353 K overnight.

2.3. Characterization of sponges

To obtain the Fourier Transform Infrared Spectroscopy (FTIR) spectra and identify the functional groups present in Sponge, MPA@Sponge, and Cys@Sponge; FTIR equipped with Attenuated Total Reflectance (ATR) module (ATR-FTIR, Tensor 27, Bruker, Germany) was utilized. The quantification of sulfur content was performed utilizing an element analyzer (Flash EA 2000 CHNS, Thermo Fisher, America). The point of zero charge (pH_{pzc}) of sponges were measured using pH drift method [36]. Specifically, pH_{pzc} was determined using 0.1 $mol \cdot L^{-1}$ NaCl solutions spanning pH 2–9. pH adjustments were achieved using either 0.1 $mol \cdot L^{-1}$ HCl or 0.1 $mol \cdot L^{-1}$ NaOH solutions. A total of 20 mL of each solution was brought into contact with 0.1 g of the sample, followed by 24 h of stirring. Subsequently, the sponge was separated via filtration, and the pH of the filtrate was measured. The pH_{pzc} value was obtained by plotting the initial pH of solution against the difference in pH values. The morphological analysis of the sponges was performed using a Field Emission-Scanning Electron Microscope (FE-SEM, MERLIN, Zeiss) with a resolution of 1.4 nm at 1 kV. The probe current ranges from 4 pA to 100 nA, while the accelerating voltage varies from 0.2 to 30 kV. The specific surface areas of sponges were determined using N_2 adsorption–desorption experiments conducted on a Micromeritics ASAP 2460 analyzer at a temperature of 77 K. All sponges were degassed 12 h under

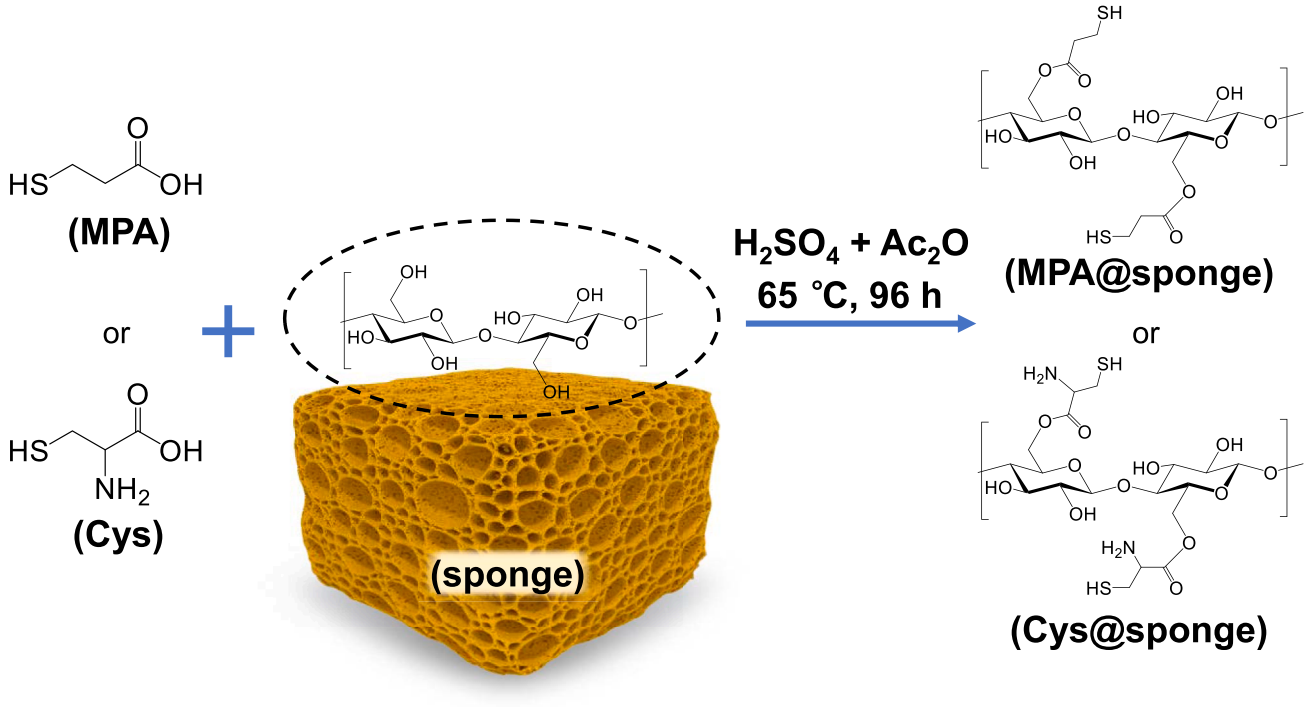

Fig. 1. Schematic illustration of the preparation procedure for MPA@Sponge and Cys@Sponge.

a vacuum at 423 K before the measurement. The specific surface area was calculated utilizing the Brunauer-Emmett-Teller (BET) method.

2.4. Batch adsorption Pt-CDs

The adsorption behavior of cisplatin and carboplatin was investigated under different experimental conditions, including pH (ranging from 2 to 6), contact time (from 1 min to 24 h), initial concentration (varying from 47 $\mu g{\cdot}L^{-1}$ to 500 $mg{\cdot}L^{-1}$, expressed as Pt for both Pt-CDs), and solution temperature (293, 318, and 343 K). The pH of the solution was controlled by using 0.1 $mol{\cdot}L^{-1}$ NaOH and/or 0.1 $mol{\cdot}L^{-1}$ HCl to achieve the desired pH, which was monitored using a pH meter (Crison, Spain) prior to, during, and after the adsorption. Batch adsorption experiments were conducted by adding 10 mg of the adsorbent to 2 mL of Pt solution (either cisplatin or carboplatin) in a plastic centrifuge tube. The mixture was subjected to mechanical agitation at 300 rpm at a specific temperature. Following a predetermined duration, typically 24 h (except in the case of kinetic studies), the adsorbent was separated from the solution by a 0.22 μm membrane filter. The remaining Pt concentration of the filtrate was quantified by means of Inductively Coupled Plasma Mass Spectrometry (ICP-MS, Thermo XSeries II, Thermo Scientific, USA).

The equilibrium adsorption capacity q_e ($\mu g{\cdot}g^{-1}$) of Pt was determined by applying Eq. (1):

$$q_e = \frac{(c_0 - c_e)}{m} \times V \tag{1}$$

where c_0 and c_e represent the initial and equilibrium Pt concentrations ($\mu g{\cdot}L^{-1}$), respectively, V indicates the volume of solution (mL), and m denotes the adsorbent dosage (mg). In the case of kinetic studies, c_e is substituted by the remaining Pt concentration at time t, c_t ($\mu g{\cdot}L^{-1}$), to calculate the corresponding adsorption capacity (q_t, $\mu g{\cdot}g^{-1}$).

Subsequently, the removal ratios were determined by Eq. (2):

$$\text{Removal ratio} = \frac{(c_0 - c_e)}{c_0} \times 100\% \tag{2}$$

All adsorption experiments were performed in triplicate, and the average along with the corresponding relative standard deviations were computed.

To fully comprehend the adsorption behaviour of Pt-CDs, fitting analysis was conducted on the adsorption data collected at different contact time using pseudo-first-order (PFO) and pseudo-second-order (PSO) kinetic models. Additionally, isotherm models such as Langmuir and Freundlich were employed to fit the data derived from diverse initial concentrations. All chosen model formulations are described in Supplementary data.

2.5. Synchrotron X-ray absorption spectroscopy (XAS)

X-ray absorption spectroscopy (XAS) experiment was carried out at BL22 CLÆSS beamline of ALBA CELLS synchrotron [37]. Pt L_3-edge XAS measurements were conducted to investigate the chemical state and coordination environment of adsorbed cisplatin and carboplatin. The measurements were collected on adsorbents that had been exposed to an initial concentration of 235 $\mu g{\cdot}L^{-1}$ Pt. Samples were pressed into a 13 mm pellet to facilitate handling. A Si(311) double crystal monochromator was employed for the measurements. The measurements were performed at a temperature of liquid nitrogen to mitigate potential radiation-induced damage. Given the relatively low Pt concentration in the samples, the measurements were conducted in fluorescence mode utilizing a multi-element silicon drift detector equipped with Xspress3 electronics.

Solid Pt references (K_2PtCl_4, cisplatin, carboplatin) were measured in transmission mode at room temperature, and their solutions in different mediums (cisplatin in 0.2 $mol{\cdot}L^{-1}$ HCl, carboplatin in 0.2 $mol{\cdot}L^{-1}$ HCl and Milli-Q water, Pt concentration of 100 $mg{\cdot}L^{-1}$) were loaded into the in-house designed 3D-printed liquid cell [38] and then collected in fluorescence mode at room temperature.

The X-ray absorption near edge structure (XANES) data were subjected to normalization and background subtraction procedures utilizing the Athena software, while the extended X-ray Absorption fine structure (EXAFS) data were processed through the Artemis software [39]. The pseudoradial distribution functions presented as the module of the Fourier transform of the EXAFS signal are not phase-shift corrected.

2.6. Removal of Pt-CDs from urine and diluted urine

The study intended to assess the feasibility and effectiveness of thiol functionalized sponge in eliminating cisplatin and carboplatin from urine. Experiments were conducted using spiked urine samples obtained from a healthy male, as collecting urine samples from patients undergoing Pt cytostatic treatment proved challenging. The spiked samples used in the study consisted of cisplatin, carboplatin, and their mixtures. Each sample had an initial total Pt concentration of 235 $\mu g{\cdot}L^{-1}$, which closely resembled the concentrations typically found in hospital wastewaters. Additionally, to assess the matrix effect and simulate possible dilution in hospital wastewater, the same procedure was applied to urine samples diluted ten-time and 100-time using tap water. Ion chromatography (Dionex Aquion, Thermo Scientific, America) was chosen as the analytical technique for quantifying the levels of commonly occurring cations and anions in urine samples as well as two synthetic analogues of hospital wastewater, and further information can be found in the Table S6 in Supplementary data.

Subsequently, 10 mg of the chosen adsorbent was added to 2 mL of the Pt-spiked urine samples, and the mixture was continuously stirred for 24 h at 343 K. The resultant samples were then filtered via 0.22 μm filters before being collected using sterile plastic bottles. The Pt concentration of the samples was subsequently determined using a standardized analytical technique that has been detailed in previous literature [40,41]. In detail, a 100 μL sample was subjected to equilibration at room temperature and then was digested with 200 μL of HNO_3 (69.0–70.0%, for trace metal analysis), at a temperature of 363 K for 1 h. The resultant digested samples were then diluted to a final concentration of 2% v/v HNO_3 by diluting to 10 mL with Milli-Q water. The concentration of Pt was immediately determined by ICP-MS, with external calibration over a concentration range of 1 to 150 $\mu g{\cdot}L^{-1}$. Indium (In) and Rhodium (Rh) were employed as internal standard elements. Then the removal ratio was determined by Eq. (2).

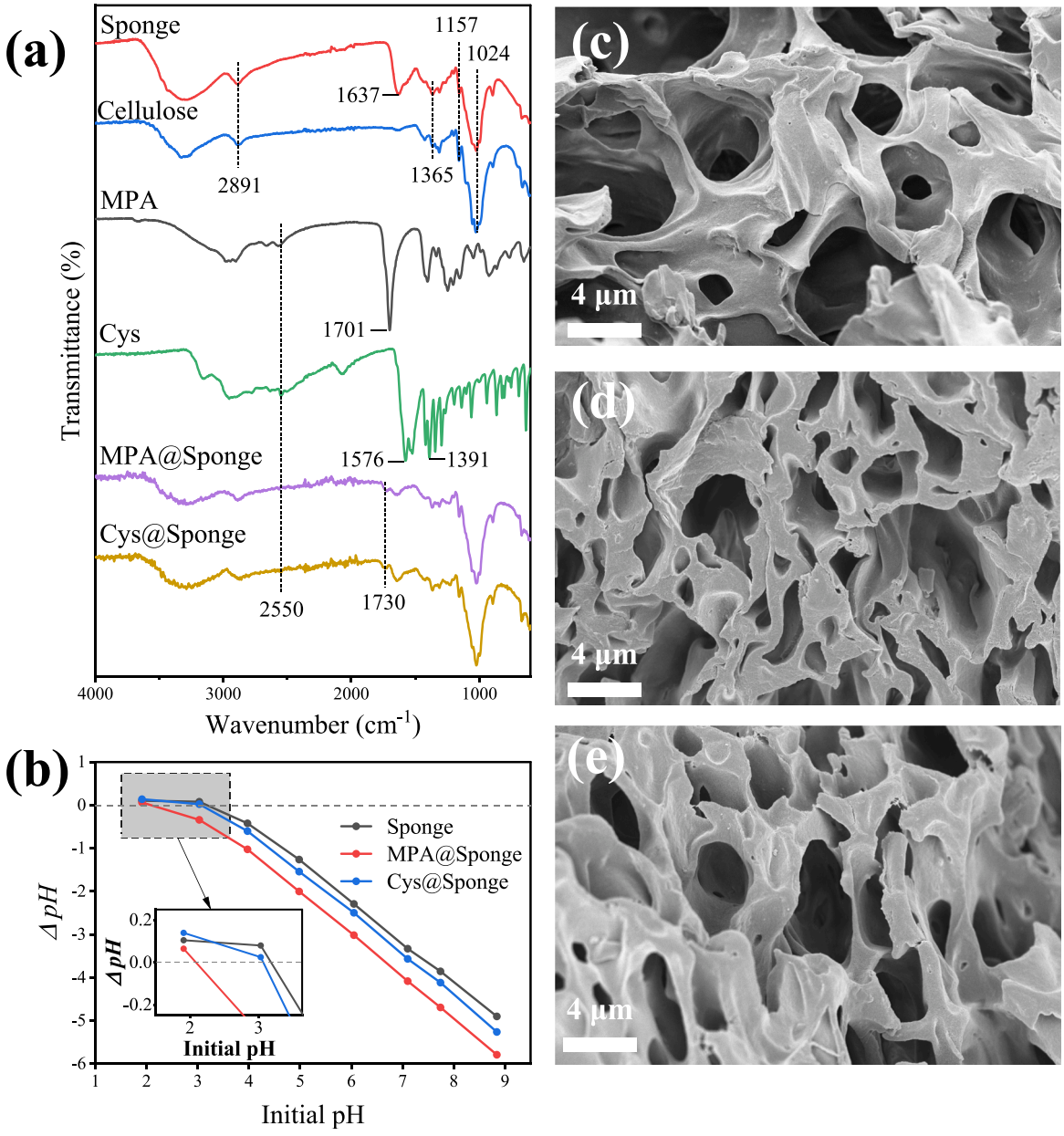

Fig. 2. (a) FTIR spectra of Sponge, cellulose, MPA, Cys, MPA@Sponge, and Cys@Sponge; (b) pH_{pzc} determination of Sponge, MPA@Sponge, and Cys@Sponge by pH drift method; SEM images of (c) Sponge, (d) MPA@Sponge, and (e) Cys@Sponge.

3. Results and discussion

3.1. Characterization of sponges

Fig. 2a presents the spectra resulting from the FTIR analysis of Sponge, cellulose, MPA, Cys, MPA@Sponge and Cys@Sponge. Relevant patents and studies [42–47] suggest that the porous cellulose sponge is composed of a thermally induced amide-forming, insoluble, water-swellable polymer, polyethyleneimine, physically bound to the sponge (see in Fig. S1). This polymer product is claimed to exhibit high affinity for the adsorption of transition metal ions [42–47]. Regarding Sponge, compared to pure cellulose, the FTIR analysis revealed absorbances at 3435, 2891, 1365, 1157, and 1024 cm^{-1}, which can be attributed to the cellulose substrate [48]. The notable absorption band observed at a wavenumber of 3435 cm^{-1} can be ascribed to the stretching vibration of the O-H bond. This band is broader in Sponge than in cellulose, which is attributed to the overlap of the band corresponding to N-H stretching vibrations. This feature is ascribed to the polyethyleneimine on the surface of the Sponge. Alkanes C-H bond stretching vibration is responsible for the peak with a center value of 2891 cm^{-1}. The absorption band observed at a wavenumber of 1365 cm^{-1} is assigned to the bending of the O-H bond, whereas the peak observed at 1157 cm^{-1} corresponds to the antisymmetric stretching of the C-O-C bridge. The prominent peak recorded at a wavenumber of 1024 cm^{-1} arises due to the skeletal vibration of the C-O-C pyranose ring [48]. Moreover, the absorption spectrum of Sponge exhibits an additional peak at 1637 cm^{-1}, in contrast to cellulose, and can be assigned to the stretching vibration of the C = O bond. Additionally, the peak experiences a shift towards higher wavenumbers (due to the electron-donating characteristics of nitrogen), indicating the presence of an amide structure in the polymer formed through the reaction between nitrilotriacetic acid and polyethyleneimine.

Both functionalization reagents exhibit a modest absorption peak of around 2550 cm^{-1}, which is associated with the S-H bond stretching vibration. In addition, MPA also exhibits an absorption peak at 1701 cm^{-1}, which is due to the stretching vibration of the C = O bond in the carboxyl group [49]. In contrast, the spectrum of Cys exhibits two distinct peaks at 1576 and 1391 cm^{-1}, which are attributed to the asymmetric and symmetric stretching vibrations of carboxyl (–COO-) groups, respectively [50–53]. The limited loading of the functionalized sponges resulted in the almost negligible presence of the characteristic peaks of thiols at 2550 cm^{-1}. However, the detection of a new peak at 1730 cm^{-1} in MPA@Sponge and Cys@Sponge spectra, which is attributed to the C = O stretching vibration of the ester group, serves as evidence for successful esterification. Stated differently, the anchoring of MPA and Cys on the substrate was accomplished successfully. And, similar FTIR spectral characteristics were also presented in different studies on thiol-functionalized cellulose materials [34,35,54–56].

As listed in Table S1, elemental analysis (EA) measurements showed that 1.23 ± 0.07 and 0.59 ± 0.03 wt% of sulfur were present in MPA@Sponge and Cys@Sponge after functionalization, respectively. These results also validate the successful anchoring of MPA and Cys on the substrate, as the sulfur content in the original sponge is negligible. The lower sulfur content observed in Cys@Sponge after functionalization is attributed to the necessity of employing less Cys compared to MPA, due to the low solubility of Cys in Ac_2O medium. According to Fig. 2b, the pH_{pzc} values of Sponge, MPA@Sponge, and Cys@Sponge are approximately 3.2, 2.1, and 3.1, respectively. Therefore, when the solution pH is lower than these values, the surface of the sponges will become positively charged, primarily due to the protonation of amino groups [57]. As depicted in Fig. 2c-e, all sponges demonstrate a porous structure featuring an intricate network of interconnected channels with diameters ranging approximately from 1 to 5 μm. Furthermore, after modification, these pore characteristics are retained. The N_2 adsorption–desorption isotherms are illustrated in Fig. S2, and the BET specific surface areas of Sponge, MPA@Sponge, and Cys@Sponge were determined to be 1.55, 1.66, and 1.65 $m^2 \cdot g^{-1}$, respectively.

3.2. Adsorption of Pt-CDs

3.2.1. Effect of pH values

The pH value is a crucial parameter governing the interaction between adsorbate and adsorbent. Through protonation or deprotonation processes, it can induce changes in surface charge, thereby affecting the adsorption efficiency. Additionally, in the case of Pt-CDs, the pH also impacts the hydration of Pt complexes.

Upon comparing the adsorption capacity of the sponge before and after functionalization shown in Fig. 3, it becomes apparent that the adsorption of the two Pt-CDs was enhanced when MPA and Cys were introduced. According to HSAB theory [31], Pt (II) exhibits characteristics of a “soft” acid, displaying a pronounced propensity for forming stable complexes with sulfur donors, which are classified as “soft” bases. Notably, the improvement observed in the case of MPA@Sponge is markedly superior to that observed in the case of Cys@Sponge. This is because MPA@Sponge has a higher sulfur loading rate than Cys@Sponge, as shown by EA (1.23 ± 0.07 and 0.59 ± 0.03 wt% of sulfur content in MPA@Sponge and Cys@Sponge, respectively), providing more adsorption sites. Moreover, it has been proposed that the three sponge materials demonstrated superior capabilities in the adsorption of cisplatin compared to carboplatin. This distinction can be attributed to the inherent tendency of cisplatin to undergo hydration. The dissimilarity arises from the differences between the chloride ligands of cisplatin and the bidentate chelated ligand 1,1-cyclobutanedicarboxylato (CBDCA) of carboplatin. Specifically, the chloride ligands of cisplatin are more prone to hydration, while the CBDCA ligand of carboplatin exhibits lesser susceptibility to hydration [58–63]. Consequently, the hydration-resistant nature of carboplatin impedes the substitution by the thiol group, leading to the observed disadvantage in adsorption capacity.

The impact of pH on the adsorption of cisplatin onto the three sponges is evident from the findings illustrated in Fig. 3a. As the pH value rises, a slight increase in cisplatin adsorption can be observed. This observation can be attributed to the favourable influence of high pH levels and low Cl^- concentration on the hydration of cisplatin, thereby enhancing its reactivity and facilitating complexation with the sponges [28,64–68]. The impact of pH variation on carboplatin adsorption is negligible (see Fig. 3b), except for pH 2, wherein MPA@Sponge exhibits a higher adsorption capacity compared to the values obtained at other pH values. The observed phenomenon is attributed to the introduction of additional HCl at a pH of 2, resulting in partial displacement of CBDCA ligand on carboplatin, and rendering its molecular conformation more similar to that of cisplatin, and this transformation has been already detected by chromatography [61] and XAS techniques [69].

3.2.2. Adsorption kinetics

The kinetic parameter plays a pivotal role in assessing the efficiency and mechanism of adsorption processes, which is a critical aspect to consider when scaling up Pt-CDs removal for industrial applications. The adsorption kinetic curves for cisplatin and carboplatin onto Sponge, MPA@Sponge, and Cys@Sponge are presented in Fig. 4. The results demonstrate rapid adsorption kinetics for all materials. During the initial few minutes, there is a notable rise in adsorption capacity as a result of the ample presence of active adsorption sites on the surfaces of sponges. However, as the adsorption proceeds, the growth rate progressively decelerates until it reaches equilibrium after approximately 3 h. This is primarily due to the decrease in available active sites, resulting in a reduction in the rate of adsorption. Despite its fast kinetics, the adsorption of carboplatin exhibits certain limitations when compared to that of cisplatin. As depicted in Fig. 4, the adsorption capacities (at 24 h) of MPA@Sponge and Cys@Sponge for carboplatin were merely 6.3 ± 0.8 and 5.7 ± 0.1 $\mu g \cdot g^{-1}$, respectively, compared to 29.8 ± 0.1 and 21.4 ± 0.3 $\mu g \cdot g^{-1}$ for cisplatin. Similar behavior was also observed in the

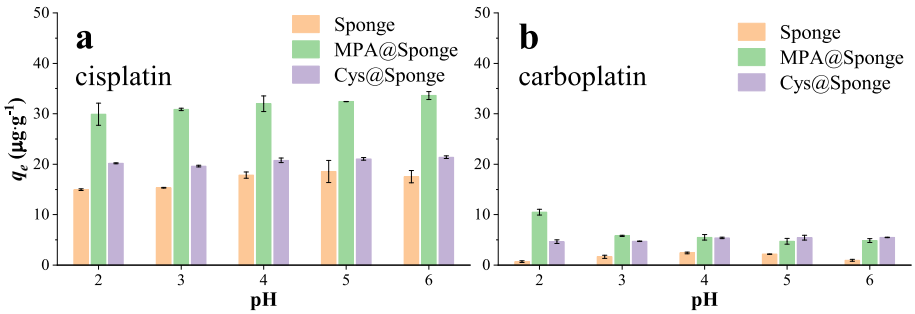

Fig. 3. pH effect on adsorption capacities of sponges on (a) cisplatin and (b) carboplatin.

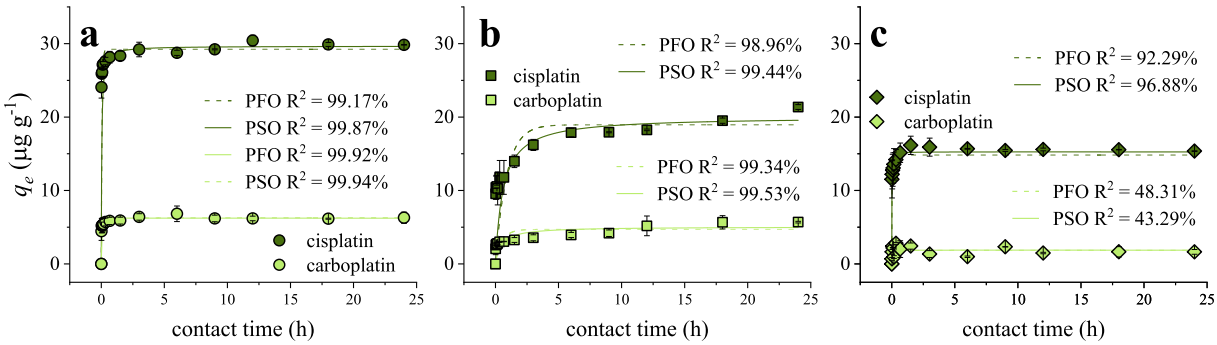

Fig. 4. Adsorption capacities of (a) MPA@Sponge, (b) Cys@Sponge, and (c) Sponge on cisplatin and carboplatin at different contact time.

adsorption on Sponge (Fig. 4c). As previously explained, this can be attributed to the low hydration rate of carboplatin.

It can be concluded that the PSO model was more suitable for fitting the data than the PFO model based on the coefficients of determination R^2 shown in Table S2 (see Supplementary data). The PSO model postulates that the rate-limiting step entails chemisorption, involving valence forces that result from the electrons sharing or exchanging between the adsorbent and adsorbate [36,70,71]. On the other hand, the PFO model is suitable for characterizing the early phase of adsorption, wherein the rate-controlling step is external/internal diffusion, and the adsorbate typically exhibits a high initial concentration [70,72]. On the contrary, the present study involved a low initial concentration (235 μg·L^{-1}) of the target Pt-CDs and an abundance of active sites in the adsorbents. This scenario signifies that the adsorption is primarily governed by the bonding process of the adsorbate to the active sites, thus aligning with assumptions of the PSO model.

3.2.3. *Adsorption isotherms*

Adsorption isotherm characterizes the equilibrium relationship between the adsorbate present in the liquid phase and the adsorbate adsorbed on solid adsorbent at constant temperature [73]. Fig. 5 illustrates an increase in adsorption capacity as the initial concentration increases. This phenomenon can be accounted for by the presence of a higher concentration gradient occurring at the interface between the solid and liquid phases, which drives the mass transfer of Pt-CDs towards the adsorbent surface, which satisfies the generalized Fick Law [74,75].

By comparing the adsorption isotherms at varying temperatures, a discernible increase in adsorption can be observed with rising temperature. Nevertheless, distinct patterns can be observed in the impact of temperature on the adsorption processes of cisplatin and carboplatin. It has been observed that the adsorption of cisplatin proportionally increases with the temperature rise (left column in Fig. 5). The observed phenomenon is ascribed to the temperature-favoured complexation of the center Pt of cisplatin with thiol groups present on the surfaces of the MPA@Sponge and Cys@Sponge, and the same explanation also applies to the adsorption of carboplatin. In contrast, as illustrated in the right column of Fig. 5, a slight increase in the adsorption capacity of carboplatin was observed as the temperature was elevated from 293 K to 318 K. However, an appreciable enhancement in the adsorption capacity was noted upon further raising the temperature to 343 K, particularly within the lower concentration regime, as depicted in Fig. 5d and h. As shown in another study [76], comparable distinctions were also noted during an investigation of the impact of temperature on the interplay between cisplatin and carboplatin with cellular DNA [76]. It can be explained that the influence of temperature on the adsorption of carboplatin is not only reflected in the promotion of complexation of Pt-S, but it also has a notable effect on the hydration of carboplatin [77], which is crucial to the complexation process that follows. It can be inferred that when the temperature rose to 318 K, the bidentate-chelated CBDCA of carboplatin, hindered the subsequent ligand replacement conferring carboplatin resistance to hydration. However, at 343 K, the CBDCA ring was opened and hydrated [77], resulting in derivatives with greater activity. Consequently, the adsorption of carboplatin was significantly enhanced, to a degree comparable to that of cisplatin (as evidenced by the comparison displayed in Fig. 5c and d at 343 K).

Fig. 5 also depicts the fitting curves for the adsorption processes, while Table S3 (Supplementary data) summarizes the parameters derived from the isotherm models used. By comparison, the coefficient of determination for the Langmuir model ($R^2 > 0.96$) typically surpasses that of the Freundlich model, thereby suggesting a superior fit of the Langmuir isotherm model to the experimental data, except for adsorption of cisplatin on MPA@Sponge at 318 K, where the Freundlich model shows slightly better fitting. These findings suggest that the adsorption of two Pt-CDs by MPA@Sponge and Cys@Sponge occurs via monolayer adsorption. Furthermore, in the low concentration range (Fig. 5c, d, g and h), the adsorption isotherms exhibit linear characteristics, consistent with the description of Henry's law, thereby indicating a monolayer adsorption as well [78]. The Langmuir separation factor R_L values for both Pt-CDs adsorptions on the two materials, within the concentration range investigated, range from 0 to 1, demonstrating favourable adsorption. The theoretical maximum adsorption capacities (q_m) estimated by the Langmuir model closely approximates, albeit slightly

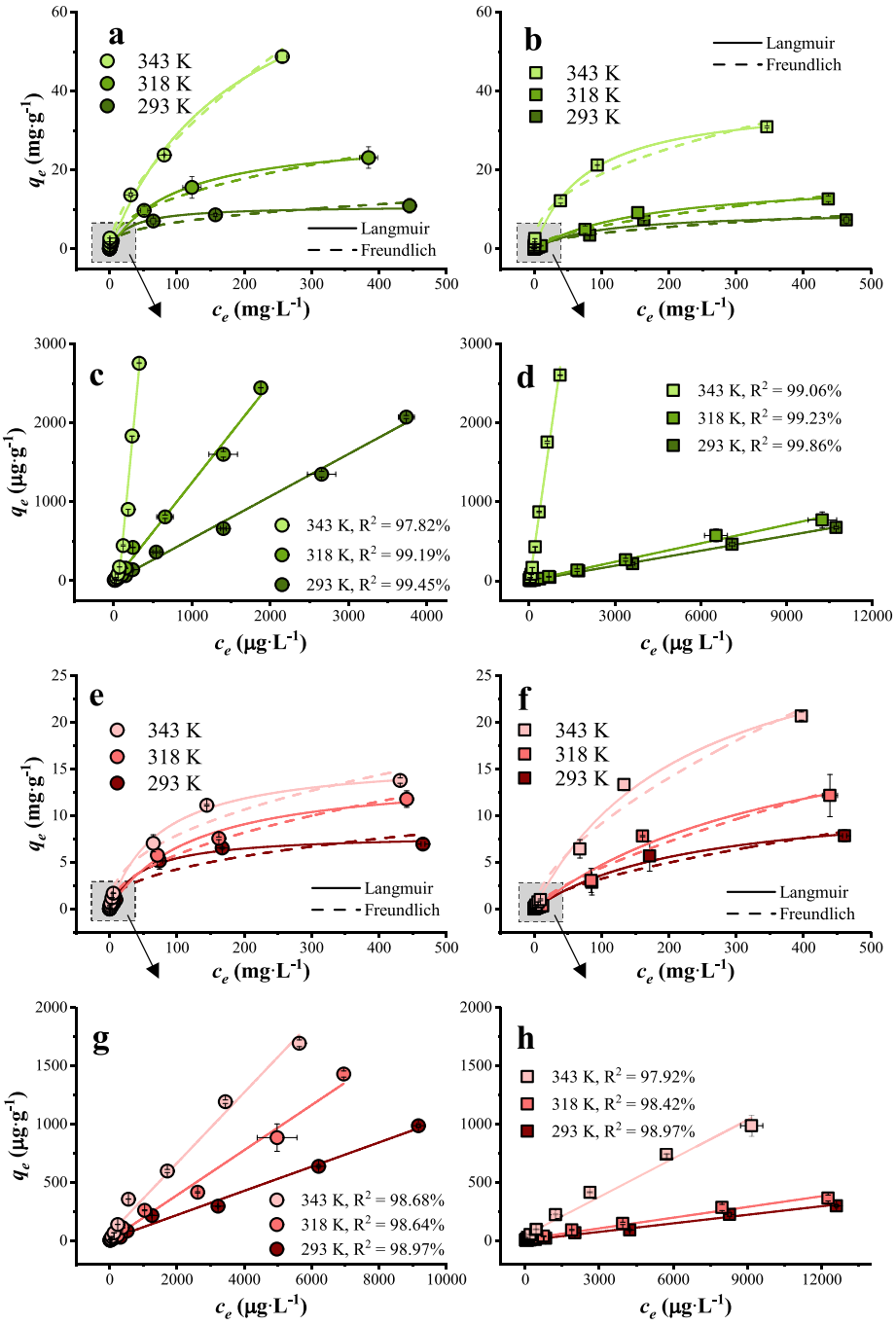

Fig. 5. Adsorption equilibriums of (a) cisplatin on MPA@Sponge, (b) carboplatin on MPA@Sponge, (e) cisplatin on Cys@Sponge and (f) carboplatin on Cys@Sponge and isotherm models fitting. Fig. (c), (d), (g) and (h) below each depict the magnified interval (with an initial concentration range of 47–14100 μg·L^{-1}).

exceeds, the experimentally obtained actual maximum adsorption capacities. The favourable nature of all adsorption processes is indicated by the Freundlich constant, as the value of $1/n$ is less than 1.

3.2.4. *Adsorption thermodynamics*

To further understand adsorption characteristics, experimental thermodynamic studies were carried out at various temperatures. The impact of temperature on the adsorption efficacy of unfunctionalized and functionalized sponges is divergent. The experimental findings presented in Fig. 6 show that the thiol-modified sponges display a temperature-favoured behaviour. Conversely, the original sponge exhibits an adsorption trend that initially increases with temperature, but subsequently decreases. It can be readily comprehended that the chemisorption processes of Pt-CDs on MPA@Sponge and Cys@Sponge were primarily governed by chelation, which exhibited a thermophilic nature. Thus, it was observed that high temperatures promoted the complexation reaction between Pt and S originating from the thiol group. However, the adsorption capacities of Pt-CDs on Sponge were only found to increase with an increase in temperature from 293 K to 318 K. This limited increase was attributed to the promotion of complexation between Pt and the amine groups on Sponge surface at 318 K. However, it is worth noting that the complexation was limited d due to the inherent "hard" basic character of N and its relatively lower bonding affinity with the "soft" acid Pt, as compared to S [31,79,80]. The adverse effects of reduced van der Waals adsorption become more pronounced when the temperature is further elevated to 343 K, resulting

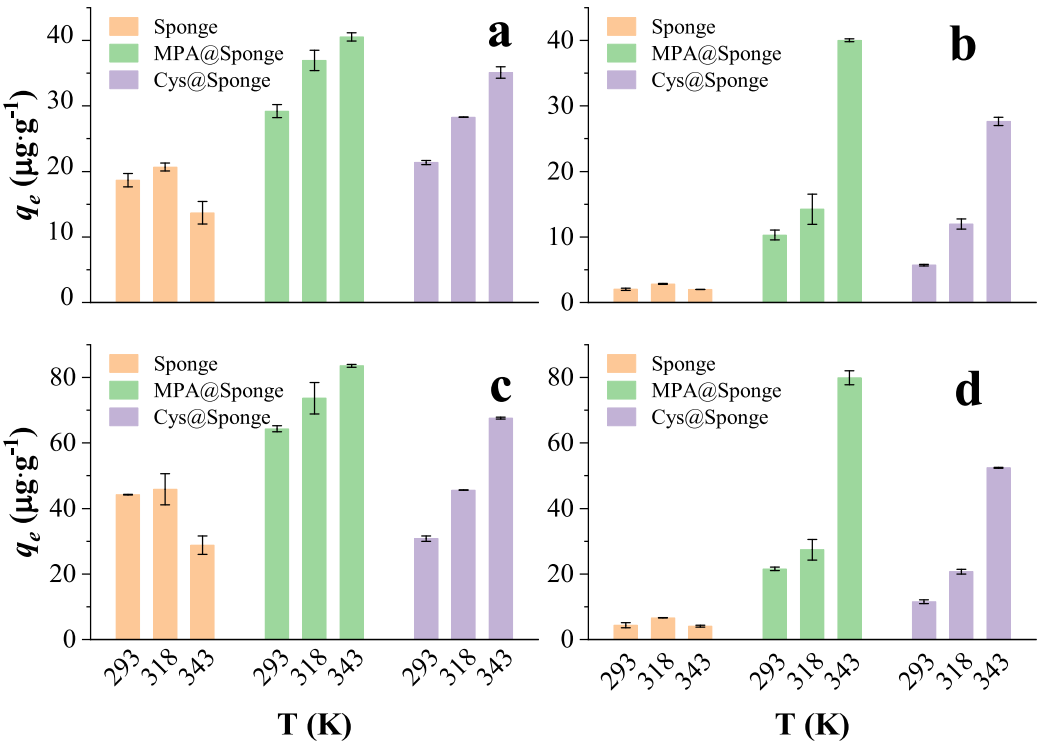

Fig. 6. Effect of temperature on the adsorption capacity of cisplatin and carboplatin. Initial Pt concentration of cisplatin: (a) 235 μg·L^{-1} and (c) 470 μg·L^{-1}; of carboplatin: (b) 235 μg·L^{-1} and (d) 470 μg·L^{-1}.

in a decline in adsorption capacity. [81]. Moreover, upon comparing the adsorption of cisplatin and carboplatin on functionalized sponges, it is noteworthy that the role of temperature in enhancing the process manifests itself in distinct manners. Specifically, while the adsorption of cisplatin exhibits a gradual increase with each increment in temperature, the adsorption of carboplatin experiences a substantial surge only when the temperature surpasses the threshold of 318 K. This observation suggests that the impact of temperature on carboplatin extends beyond the complexation reaction to other associated processes. For instance, the promotion of hydration due to an increase in temperature, as previously described, facilitates the pre-morphological transformation of carboplatin.

Furthermore, the determination of three fundamental thermodynamic parameters, namely ΔG° (Gibbs free energy), ΔH° (enthalpy change), and ΔS° (entropy change), was carried out using the equations detailed in the Supplementary data.

The values of ΔG° presented in Table S4 indicate that the adsorption process of cisplatin onto the two modified sponges was predominantly spontaneous, except for Cys@Sponge at a temperature of 293 K. Conversely, the adsorption of carboplatin was found to be non-spontaneous, only except at highest 343 K, where the system exhibited an energy gain from the surroundings [82–85]. Moreover, the ΔG° values exhibited a decrease as the temperature increased, suggesting that higher temperatures promote the spontaneity of adsorption [86]. The adsorption of cisplatin or carboplatin is an endothermic process based on positive ΔH° values. Additionally, a comparison of the ΔH° of cisplatin and carboplatin reveals a significant difference between the two compounds. Specifically, the adsorption of cisplatin is generally characterized by a lower energy requirement, which is consistent with previous explanations. On the other hand, the adsorption of carboplatin is hindered by a higher heat threshold, necessitating the promotion of carboplatin hydration to facilitate its activation for subsequent adsorption processes.

The positive value of the change in standard entropy (ΔS°) suggests an enhanced inclination towards disorder at the interface between the solid and solution phases during the adsorption process of Pt-CDs onto MPA@Sponge and Cys@Sponge. The process of binding Pt-CDs onto a sponge surface should be associated with a decrease in entropy due to the restriction on their conformational space, which consequently resulted in a negative contribution to the ΔS°. However, the restricted degree of freedom of Pt-CDs in solution implies that their entropy change upon adsorption is comparatively low when compared to that of water. Evidently, the positive contribution to ΔS° is a result of water molecules being excluded from the hydration layers of both the sponges and Pt-CDs upon adsorption. The exchange of molecules between the Pt-CDs and functional groups on the sponge surface facilitates the liberation of water molecules, resulting in an increase in disorderliness at the solid/fluid interface [83]. Similar results were also found in other studies using cellulose [87] or lignocellulosic waste [88] as adsorbents.

3.3. X-ray absorption spectroscopy of adsorbed Pt-CDs

The findings derived from the batch adsorption experiments conducted at the macro scale reveal that the adsorption behaviour of trace Pt-CDs follows a chemisorption mechanism, which dependents on the formation of Pt-S bonds. However, to gain deeper insights into the molecular-level adsorption process regarding the coordination environment and the chemical state of Pt in the adsorbed Pt-CDs, Pt L_3-edge XAS measurements were performed.

Fig. 7a presents Pt L_3-edge XANES spectra of Pt-CDs adsorbed on the different sponges, along with Pt(II) reference compounds (K_2PtCl_4, cisplatin, and carboplatin). Generally, the XANES spectra of the adsorbed Pt resemble those of the Pt(II) standards, albeit with slight deviations in the configuration of the white line, demonstrating the unchanged Pt valence. Consequently, unaltered Pt valence indicated the adsorption of Pt-CDs onto sponges did not entail any oxidation or redox reaction. The spectral profiles of cisplatin and carboplatin absorbed by functionalized sponges are very similar. The temperature of adsorption only affects the intensity of the white-line in the case of MPA@Sponge. However, the adsorbed Pt-CDs at low temperature manifests more noise

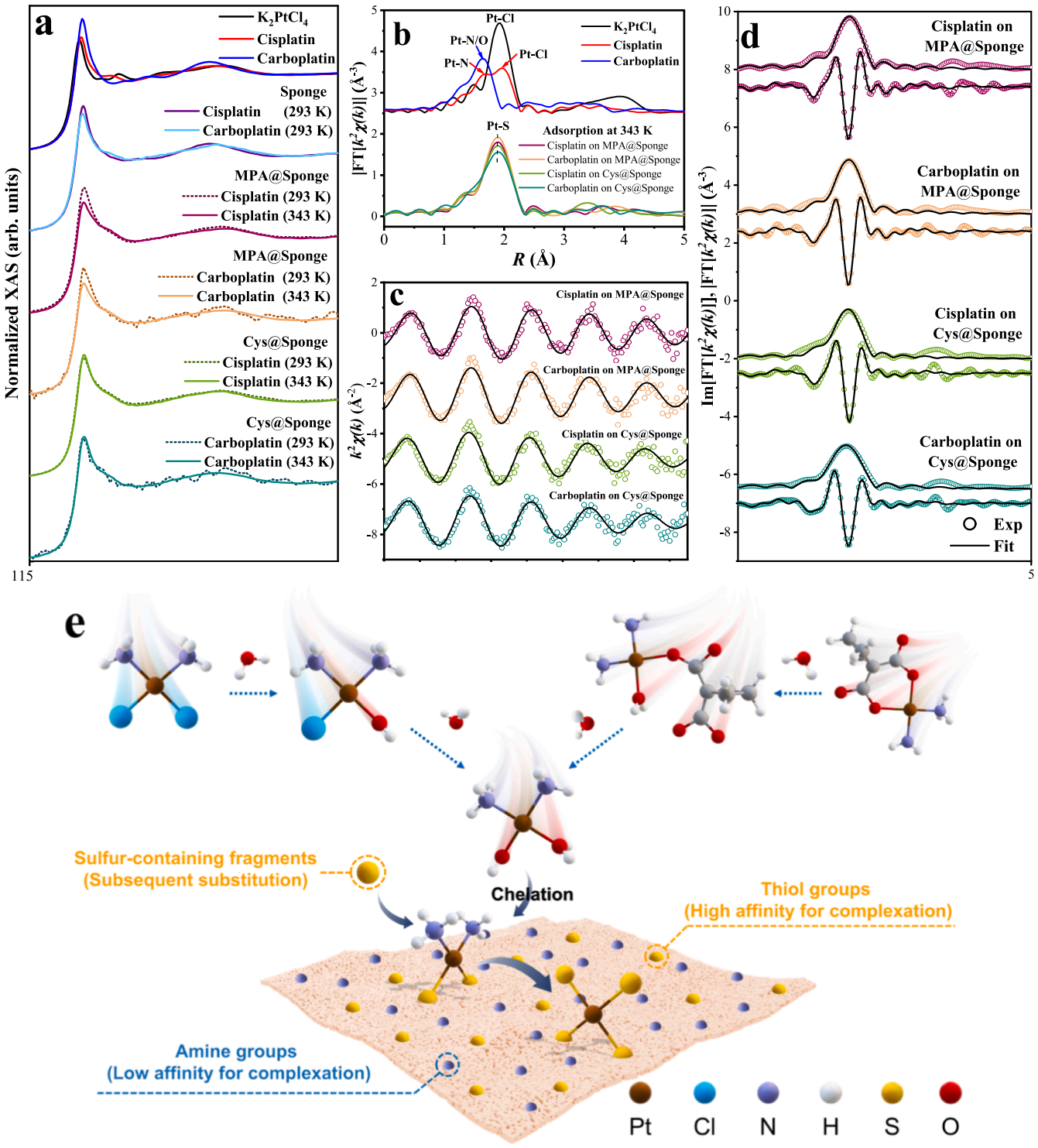

Fig. 7. Pt L_3-edge (a) XANES spectra, (b) module of the Fourier transformed EXAFS signal of Pt references (K_2PtCl_4, cisplatin and carboplatin in solid) and Pt-CDs adsorbed on sponges, (c) EXAFS signals, (d) imaginary part and module of the Fourier transformed EXAFS of Pt-CDs adsorbed on sponges at 343 K (the line represents the best fit), (e) schematic representation of Pt-CDs adsorption mechanisms by thiol-functionalized sponges.

due to the low adsorption capacities. The presence of inherent noise in low Pt-loaded samples posed a challenge for the identification of oscillations, thus EXAFS fitting analysis was feasible only on samples obtained at high-temperature adsorption. Fig. 7b depicts the module of the Fourier transformed (FT) EXAFS signal, which offers valuable insights into the coordination environment of adsorbed Pt. The dominant shell of Pt-loaded on MPA@Sponge and Cys@Sponge appears at a distance and amplitude which is like the Pt-Cl contribution in the K_2PtCl_4. In our case, this can be attributed to Pt-S bond. In order to establish the Pt coordination structure, EXAFS fitting analysis was conducted. The findings revealed that, on average, each Pt atom was coordinated by approximately four sulfur atoms within the first coordination shell at ~ 2.30 Å (as illustrated in Fig. 7c and d, and presented in Table S5). These results suggest the cisplatin and carboplatin adsorption process at low

concentrations proceeds in a manner depicted by Fig. 7e. The initial stage involves hydration of both Pt-CDs, followed by complexation with the thiol groups present on the surface of functionalized sponge by activated Pt aqua-derivatives. With prolonged heating, a portion of MPA and Cys undergoes thermal decomposition (confirmed by EA, S content of MPA@Sponge and Cys@Sponge decreased about 47% and 39%, respectively, after stirring in 343 K solution without Pt for 24 h), giving rise to sulfur-containing fragments in solution, such as sulfides [89–92], which subsequently displace the ammonia ligand despite its inertness.

3.4. Effect of Cl^- presence in stock solution on carboplatin adsorption

As elaborated previously, the derivatives of cisplatin and carboplatin demonstrated a facile complexation behaviour attributed to the Pt-S bond formation after hydration activation. However, it is noteworthy that the adsorption capacity of cisplatin always surpassed that of carboplatin. The observed contrast can be attributed to the influence of distinct ligands on the hydration rate. In particular, relative to the Cl ligand present in cisplatin, the CBDCA ligand found in carboplatin demonstrated higher resistance to hydration. Consequently, CBDCA tended to remain bound, thus resulting in more pronounced steric hindrance during subsequent complexation reactions.

In order to verify the proposed hypothesis, chloride ions (at a concentration of 0.2 mol·L^{-1} in either the form of HCl or NaCl) were introduced into the stock solution of carboplatin (Pt 100 mg·L^{-1}) to expedite the hydration process of carboplatin. The adsorption experiment was conducted under identical conditions to those of the carboplatin Cl-free stock solution (initial Pt concentration of 235 μg·L^{-1} obtained through dilution of the stock solution with Milli-Q water, adsorbent dosage of 10 mg, solution volume of 2 mL, pH 3, 24 h, and 293 K). Their adsorption capacities were determined and compared, as depicted in Fig. 8a.

Upon introduction of HCl to the stored solution, there was a notable improvement in the adsorption of carboplatin by both adsorbents. Specifically, the adsorption capacity of MPA@Sponge and Cys@Sponge increased significantly from 5.8 ± 0.1 and 4.7 ± 0.1 to 13.9 ± 0.9 and 9.4 ± 0.2 μg·g^{-1}, respectively. By analyzing XANES spectra of carboplatin stocks in the presence and absence of HCl, as illustrated in Fig. 8b, it is observed that carboplatin manifests distinct spectral features compared to carboplatin in H_2O stock solution, but shares similarities with cisplatin when exposed to HCl. The mechanism of the carboplatin transformation was proposed by Curis et al., [69] to explain their XAS results on carboplatin decomposition in chloride medium. And it was also previously corroborated by chromatographic techniques [61]. It can be inferred that the stability of carboplatin was affected by this transformation (Fig. 8c), which resulted in the formation of an open-ring structure that demonstrated enhanced adsorption activity. Nonetheless, the introduction of an equivalent concentration of Cl ions in the form of NaCl to the original solution did not result in the anticipated increase in adsorption. Although a slight increase was observed with ageing of the stock up to 40 days, it suggested that acidity and Cl jointly played a crucial role in the conversion process. Similarly, Curis et al., did not find that carboplatin had the same transformation in neutral NaCl solution as in HCl solution [69].

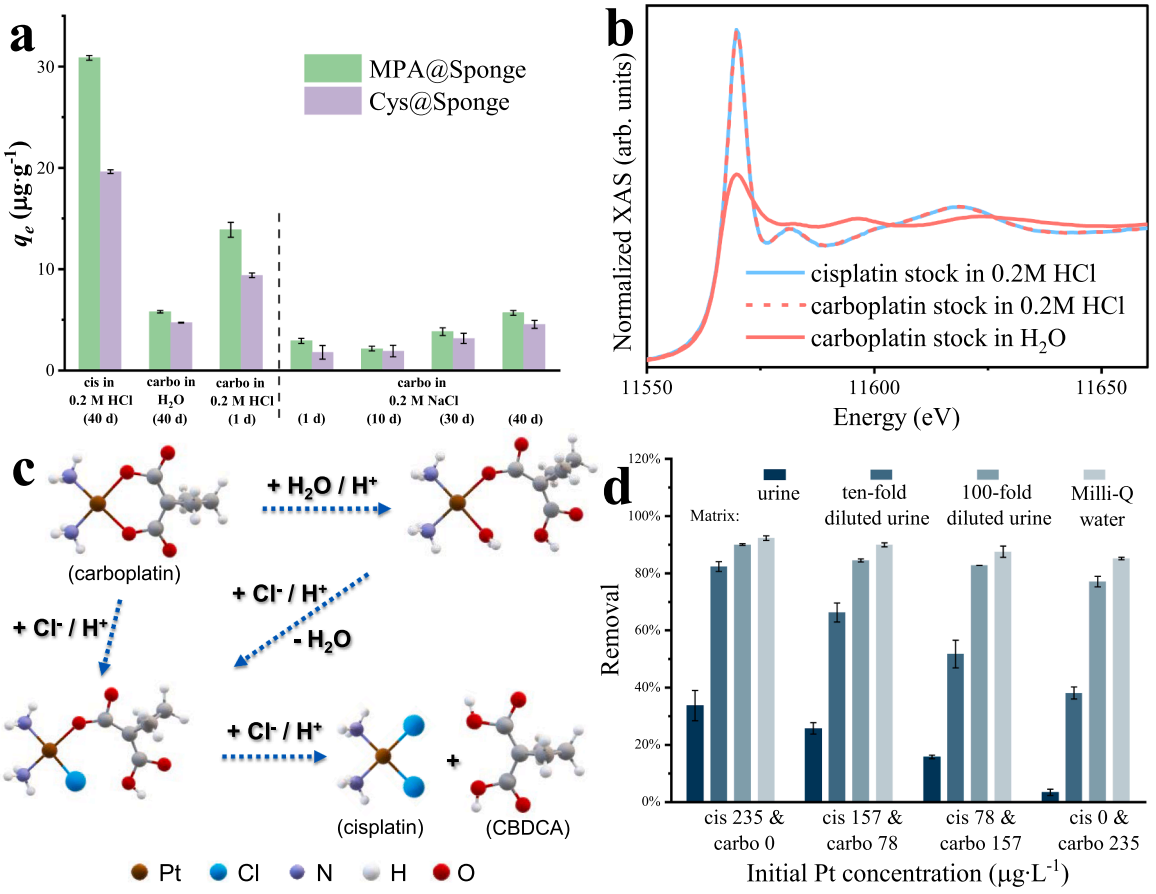

Fig. 8. (a) Effect of Cl ions in the stock solution on the adsorption capacity of carboplatin; (b) XANES spectra of cisplatin stock solution in 0.2 mol·L^{-1} HCl, carboplatin stock solution in H_2O, and cisplatin stock solution in 0.2 mol·L^{-1} HCl; (c) the transformation of carboplatin to cisplatin within an HCl-containing medium; (d) removal of cisplatin, carboplatin, and their mixtures from spiked urine samples by MPA@Sponge.

3.5. Experimental verification of Pt-CDs removal from urine and diluted urine

As present in Fig. 8d, there is a noteworthy augmentation in the adsorption capacity of MPA@Sponge towards Pt with the dilution of the urine matrix. This effect signifies a considerable reduction in the interference intensity of the matrix effect. The matrix effect observed in the experiment is unequivocally attributed to the intricate nature of the urine composition (listed in Table S6). One of the potential factors that may impede the removal of cisplatin and carboplatin is the presence of trace proteins like Tamm-Horsfall protein in urine [93,94], which contains cysteine residues that may pre-chelate a portion of these drugs. Furthermore, the presence of components like NH_4^+ and Cl^- in the urine matrix may interfere with the substitution of cisplatin and carboplatin ligands., thereby adversely affecting their complexation with the MPA@Sponge surface [40]. In addition, the coexistence of ions such as Na^+, K^+, Mg^{2+}, and Ca^{2+} in urine results in competitive adsorption, thereby slightly impeding the adsorption of cisplatin and carboplatin [95].

Additionally, the results reveal that the rise in mixed carboplatin leads to a notable reduction in the Pt adsorption capacity. Nonetheless, this declining pattern appears to mitigate in 100-fold diluted urine, whereby the reduction decreases from 90.0 ± 0.3% to 77.0 ± 0.2% while the values decrease from 34 ± 5% to 3 ± 1% in non-diluted urine and from 82 ± 2% to 38 ± 2% in ten-fold diluted urine, respectively. The present finding demonstrates that the matrix effect may exert a greater influence on the pre-hydration activation of carboplatin, in comparison to aforementioned interference factors like protein complexation and competitive adsorption which are expected to impede the adsorption of the two Pt-CDs to a similar degree. In essence, the impurities in the urine maintained the rigidity of the carboplatin structure.

3.6. Comparison of thiol-functionalized sponges with commercial adsorbents

The efficacy of MPA@Sponge and Cys@Sponge for cisplatin removal was compared with that of two commercially available adsorbents, namely 3-Mercaptopropyl-functionalized silica gel (Si-SH) and cysteine-functionalized silica gel (Si-Cys), and results were summarized in Table S7. MPA@Sponge exhibits significant efficiency in the removal process (71.5 ± 0.2%), which is comparable to Si-Cys (76.3 ± 0.2%), but noticeably lower than Si-SH (98.7 ± 0.1%). This disparity can be attributed to the much higher sulfur loading of Si-SH (4.97 ± 0.07 wt%) than that of MPA@Sponge (1.23 ± 0.07 wt%) and Si-Cys (1.30 ± 0.02 wt%). While the performance of functionalized sponges is slightly inferior to commercial adsorbents, cost considerations must be taken into account. From a cost perspective, our proposed materials offer considerable advantages. Furthermore, the removal efficiency of Si-Cys on Pt-CDs, in comparison with other reported adsorbents, has been previously published in prior research study [26].

4. Conclusions

The coupling of MPA and Cys with Sponge via a simple one-step esterification reaction has been demonstrated as a feasible and successful process. The presence of an implanted high-affinity thiol group has been demonstrated to significantly enhance the adsorption of both cisplatin and carboplatin, suggesting that Pt-S complexation plays a pivotal role in chelation-dominated chemical adsorption. Then the utilization of synchrotron XAS has enabled the investigation of the coordination environment of Pt-CDs loaded at extremely low concentrations. In particular, EXAFS analysis provides insight into the formation of Pt-S bonds after adsorption, allowing for a persuasive explanation of the molecular-level adsorption mechanism. Besides complexation, the process of removing Pt-CDs also involves a hydration process for both Pt-CDs. Pre-displacing ligands in an aqueous solution can result in the production of more active derivatives, which in turn facilitate subsequent complexation. Therefore, the distinct hydration patterns of cisplatin and carboplatin lead to the preferential adsorption of cisplatin over carboplatin. The higher hydration resistance of CBDCA ligand from carboplatin accounts for the adsorption disadvantages observed. Further elevating the temperature to 343 K promoted the adsorption of Pt-CDs by MPA@Sponge, resulting in the removal of 88.9 ± 0.5% and 85.2 ± 0.4%, respectively (while 75 ± 2% and 59 ± 1% for Cys@Sponge). This was due to the temperature-enhanced chelation reaction of Pt-S. Adsorption thermodynamic studies also confirmed that adsorption is a thermally favoured endothermic reaction. Moreover, the adsorption of both Pt-CDs conforms to the Pseudo-second-order kinetic model and the Langmuir isotherm model. In summary, the elimination of Pt-CDs at trace concentrations is associated with a hydration process and a chelation-dominant chemisorption. Significantly, the examination of the Pt-spiked urine treatment has demonstrated the potential utilization of MPA@Sponge for the purpose of treating urine samples from patients that contain cisplatin and/or carboplatin, as well as hospital wastewater contaminated with these substances. To summarize, our study has introduced innovative methods for effectively managing wastewater polluted with Pt-CDs, thereby offering a practical strategy to tackle this emerging environmental threat that has been persistently overlooked.

Declaration of Competing Interest

The authors declare that they have no known competing financial interests or personal relationships that could have appeared to influence the work reported in this paper.

Data availability

Data will be made available on request.

Acknowledgements

This study was conducted within the scope of the RECOPHARMA project (grant agreement #778266) under the European Community's H2020 Program H2020-MSCA-RISE 2017. D. Han acknowledges the support from the China Scholarships Council (No. 201906450024). The authors would like to express their gratitude to the ALBA synchrotron facility for providing beamtime (No. 2022085922) at the BL22-CLÆSS beamline, and to Carlo Marini for his assistance as the scientific local contact. The authors would like to thank Cristina Navarro Senent from the Servei de Microscòpia of Universitat Autònoma de Barcelona (UAB). All the authors are grateful to the Servei d'Anàlisi Química of the UAB for the analysis. All authors thank Yunhui Yang for his help on BET analysis. Additionally, the authors extend their appreciation to Markel Luaces, Yusleydi Enamorado, and Alejandro Barragán Beltri for their assistance during the experiment. Open Access funding provided thanks to the agreement CRUE- CSIC with Elsevier.

Appendix A. Supplementary data

Supplementary data to this article can be found online at https://doi.org/10.1016/j.cej.2023.144894.

References

[1] E. Heath, M. Isidori, T. Kosjek, M. Filipič (Eds.), Fate and Effects of Anticancer Drugs in the Environment, Springer International Publishing, Cham, 2020.
[2] T.I.A. Gouveia, A.M.T. Silva, M.G. Freire, A.C.A. Sousa, A. Alves, M.S.F. Santos, Multi-target analysis of cytostatics in hospital effluents over a 9-month period, J. Hazard. Mater. 448 (2023), 130883, https://doi.org/10.1016/j.jhazmat.2023.130883.
[3] D. Li, H. Chen, H. Liu, D. Schlenk, J. Mu, S. Lacorte, G.G. Ying, L. Xie, Anticancer drugs in the aquatic ecosystem: environmental occurrence, ecotoxicological effect

and risk assessment, Environ. Int. 153 (2021), 106543, https://doi.org/10.1016/j.envint.2021.106543.
[4] C.W.P. Schmidt, Pediatric oncologic pharmacy, springer international publishing, Cham (2019), https://doi.org/10.1007/978-3-030-10988-2.
[5] V. Queirós, U.M. Azeiteiro, A.M.V.M. Soares, R. Freitas, The antineoplastic drugs cyclophosphamide and cisplatin in the aquatic environment – review, J. Hazard. Mater. 412 (2021) 125028.
[6] M. Kundi, A. Parrella, M. Lavorgna, E. Criscuolo, C. Russo, M. Isidori, Prediction and assessment of ecogenotoxicity of antineoplastic drugs in binary mixtures, Environ. Sci. Pollut. Res. 23 (2016) 14771–14779, https://doi.org/10.1007/s11356-015-4884-x.
[7] C. Russo, M. Isidori, J.A. Deaver, H.C. Poynton, Toxicogenomic responses of low level anticancer drug exposures in Daphnia magna, Aquat. Toxicol. 203 (2018) 40–50, https://doi.org/10.1016/j.aquatox.2018.07.010.
[8] S. Kolarević, Z. Gačić, J. Kostić, K. Sunjog, M. Kračun-Kolarević, M. Paunović, J. Knežević-Vukčević, B. Vuković-Gačić, Impact of common cytostatics on DNA damage in freshwater mussels unio pictorum and unio tumidus, Clean - Soil, Air, Water. 44 (2016) 1471–1476, https://doi.org/10.1002/clen.201500482.
[9] C. Trombini, T. Garcia da Fonseca, M. Morais, T.L. Rocha, J. Blasco, M.J. Bebianno, Toxic effects of cisplatin cytostatic drug in mussel Mytilus galloprovincialis, Mar. Environ. Res. 119 (2016) 12–21, https://doi.org/10.1016/j.marenvres.2016.05.004.
[10] T.G. Fonseca, M.B. Morais, T. Rocha, D.M.S. Abessa, M. Aureliano, M.J. Bebianno, Ecotoxicological assessment of the anticancer drug cisplatin in the polychaete Nereis diversicolor, Sci. Total Environ. 575 (2017) 162–172, https://doi.org/10.1016/j.scitotenv.2016.09.185.
[11] T.G. da Fonseca, D.M.S. Abessa, M.J. Bebianno, Effects of mixtures of anticancer drugs in the benthic polychaete Nereis diversicolor, Environ. Pollut. 252 (2019) 1180–1192, https://doi.org/10.1016/j.envpol.2019.05.095.
[12] M. Jureczko, J. Kalka, Cytostatic pharmaceuticals as water contaminants, Eur. J. Pharmacol. 866 (2020), 172816, https://doi.org/10.1016/j.ejphar.2019.172816.
[13] T. Farías, S. Hajizadeh, L. Ye, Cryogels with high cisplatin adsorption capacity: Towards removal of cytotoxic drugs from wastewater, Sep. Purif. Technol. 235 (2020), 116203, https://doi.org/10.1016/j.seppur.2019.116203.
[14] F. Ogata, K. Inoue, H. Tominaga, Y. Iwata, A. Ueda, Y. Tanaka, N. Kawasaki, Use of calcined gibbsite to remove cisplatin from aqueous solutions, J. Water Environ. Technol. 12 (2014) 13–23, https://doi.org/10.2965/jwet.2014.13.
[15] K. Lenz, S. Hann, G. Koellensperger, Z. Stefanka, G. Stingeder, N. Weissenbacher, S. N. Mahnik, M. Fuerhacker, Presence of cancerostatic platinum compounds in hospital wastewater and possible elimination by adsorption to activated sludge, Sci. Total Environ. 345 (2005) 141–152, https://doi.org/10.1016/j.scitotenv.2004.11.007.
[16] K. Folens, A. Abebe, J. Tang, F. Ronsse, G. Du Laing, Biosorption of residual cisplatin, carboplatin and oxaliplatin antineoplastic drugs in urine after chemotherapy treatment, Environ. Chem. 15 (2018) 506–512, https://doi.org/10.1071/EN18115.
[17] J. Dobrzyńska, M. Dąbrowska, R. Olchowski, E. Zięba, R. Dobrowolski, Development of a method for removal of platinum from hospital wastewater by novel ion-imprinted mesoporous organosilica, J. Environ. Chem. Eng. 9 (4) (2021) 105302.
[18] K. Lenz, G. Koellensperger, S. Hann, N. Weissenbacher, S.N. Mahnik, M. Fuerhacker, Fate of cancerostatic platinum compounds in biological wastewater treatment of hospital effluents, Chemosphere 69 (2007) 1765–1774, https://doi.org/10.1016/j.chemosphere.2007.05.062.
[19] K. Lenz, S.N. Mahnik, N. Weissenbacher, R.M. Mader, P. Krenn, S. Hann, G. Koellensperger, M. Uhl, S. Knasmüller, F. Ferk, W. Bursch, M. Fuerhacker, Monitoring, removal and risk assessment of cytostatic drugs in hospital wastewater, Water Sci. Technol. 56 (2007) 141–149, https://doi.org/10.2166/wst.2007.828.
[20] C. Hernández, Y. Ramos, L.A. Fernández, O. Ledea, M. Bataller, E. Véliz, V. Besada, A. Rosado, Ozonation of cisplatin in aqueous solution at pH 9, Ozone Sci. Eng. 30 (2008) 189–196, https://doi.org/10.1080/01919510801907722.
[21] T. Kobayashi, J. Hirose, K. Sano, N. Hiro, Y. Ijiri, H. Takiuchi, H. Tamai, H. Takenaka, K. Tanaka, T. Nakano, Evaluation of an electrolysis apparatus for inactivating antineoplastics in clinical wastewater, Chemosphere 72 (2008) 659–665, https://doi.org/10.1016/j.chemosphere.2008.02.020.
[22] J. Hirose, F. Kondo, T. Nakano, T. Kobayashi, N. Hiro, Y. Ando, H. Takenaka, K. Sano, Inactivation of antineoplastics in clinical wastewater by electrolysis, Chemosphere 60 (2005) 1018–1024, https://doi.org/10.1016/j.chemosphere.2005.01.024.
[23] K.D. Lee, Y. Il Jeong, D.H. Kim, G.T. Lim, K.C. Choi, Cisplatin-incorporated nanoparticles of poly(acrylic acid-co-methyl methacrylate) copolymer, Int. J. Nanomedicine. 8 (2013) 2835–2845, https://doi.org/10.2147/IJN.S48367.
[24] B. Singh, N. Chauhan, V. Sharma, Design of molecular imprinted hydrogels for controlled release of cisplatin: evaluation of network density of hydrogels, Ind. Eng. Chem. Res. 50 (2011) 13742–13751, https://doi.org/10.1021/ie200758b.
[25] R. Lombana Fraguela, J.A. Ricardo Garcia, M.E. Villanueva Tagle, M.S. Pomares Alfonso, M. Cracchiolo, A. Kovačević, M. Tolazzi, A. Melchior, M. Sanadar, Evaluation of Dithiocarbamate-Modified Silica for Cisplatin Removal from Water, Processes. 11 (2023) 472. https://doi.org/10.3390/pr11020472.
[26] D. Han, M. López-Mesas, M. Luaces, Y. Enamorado, M. Sanadar, A. Melchior, M. Valiente, Comparative study on removal of platinum cytostatic drugs at trace level by cysteine, diethylenetriamino functionalized Si-gels and polyethyleneimine functionalized sponge: adsorption performance and mechanisms, Sci. Total Environ. 891 (2023), 164385, https://doi.org/10.1016/j.scitotenv.2023.164385.
[27] T.C. Johnstone, K. Suntharalingam, S.J. Lippard, The next generation of platinum drugs: targeted Pt(II) agents, nanoparticle delivery, and Pt(IV) prodrugs, Chem. Rev. 116 (2016) 3436–3486, https://doi.org/10.1021/acs.chemrev.5b00597.
[28] L. Kelland, The resurgence of platinum-based cancer chemotherapy, Nat. Rev. Cancer. 7 (2007) 573–584, https://doi.org/10.1038/nrc2167.
[29] B.P. Espósito, R. Najjar, Interactions of antitumoral platinum-group metallodrugs with albumin, Coord. Chem. Rev. 232 (2002) 137–149, https://doi.org/10.1016/S0010-8545(02)00049-8.
[30] A.I. Ivanov, J. Christodoulou, J.A. Parkinson, K.J. Barnham, A. Tucker, J. Woodrow, P.J. Sadler, Cisplatin binding sites on human albumin, J. Biol. Chem. 273 (1998) 14721–14730, https://doi.org/10.1074/jbc.273.24.14721.
[31] Ž.D. Bugarčić, J. Bogojeski, B. Petrović, S. Hochreuther, R. van Eldik, Mechanistic studies on the reactions of platinum(ii) complexes with nitrogen- and sulfur-donor biomolecules, Dalt. Trans. 41 (2012) 12329, https://doi.org/10.1039/c2dt31045g.
[32] Z. Wu, Z. Cheng, W. Ma, Adsorption of Pb(II) from glucose solution on thiol-functionalized cellulosic biomass, Bioresour. Technol. 104 (2012) 807–809, https://doi.org/10.1016/j.biortech.2011.10.100.
[33] Z. Li, L. Wu, H. Liu, H. Lan, J. Qu, Improvement of aqueous mercury adsorption on activated coke by thiol-functionalization, Chem. Eng. J. 228 (2013) 925–934, https://doi.org/10.1016/j.cej.2013.05.063.
[34] B. Parambath Kanoth, M. Claudino, M. Johansson, L.A. Berglund, Q. Zhou, Biocomposites from natural rubber: synergistic effects of functionalized cellulose nanocrystals as both reinforcing and cross-linking agents via free-radical thiol-ene chemistry, ACS Appl. Mater. Interfaces. 7 (2015) 16303–16310, https://doi.org/10.1021/acsami.5b03115.
[35] S.Y. Park, J.W. Chung, R.D. Priestley, S.Y. Kwak, Covalent assembly of metal nanoparticles on cellulose fabric and its antimicrobial activity, Cellul. 19 (2012) 2141–2151, https://doi.org/10.1007/s10570-012-9773-6.
[36] D. Mohan, A. Sarswat, V.K. Singh, M. Alexandre-Franco, C.U. Pittman, Development of magnetic activated carbon from almond shells for trinitrophenol removal from water, Chem. Eng. J. 172 (2-3) (2011) 1111–1125.
[37] L. Simonelli, C. Marini, W. Olszewski, M. Ávila Pérez, N. Ramanan, G. Guilera, V. Cuartero, K. Klementiev, Clæss,, The hard X-ray absorption beamline of the ALBA CELLS synchrotron, Cogent Phys. 3 (2016), https://doi.org/10.1080/23311940.2016.1231987.
[38] C. Marini, R. Boada, J. Prieto Burgos, N. Ramanan, I. García Domínguez, J. Zhao, T. T. Xiao, L. Simonelli, Low-cost vacuum compatible liquid cell for hard X-ray absorption spectroscopy, Nucl. Instruments Methods Phys. Res. Sect. A Accel. Spectrometers, Detect. Assoc. Equip. 908 (2018) 333–337, https://doi.org/10.1016/j.nima.2018.08.036.
[39] B. Ravel, M. Newville, Athena, Artemis, Hephaestus: data analysis for X-ray absorption spectroscopy using IFEFFIT, J. Synchrotron Radiat. 12 (2005) 537–541, https://doi.org/10.1107/S0909049505012719.
[40] W. Guo, Q. Zhou, Y. Jia, J. Xu, Cluster and factor analysis of elements in serum and urine of diabetic patients with peripheral neuropathy and healthy people, Biol. Trace Elem. Res. 194 (2020) 48–57, https://doi.org/10.1007/s12011-019-01747-x.
[41] Y. Gao, N. Yang, X. Yan, W. Hang, J. Xing, J. Zheng, E. Zhu, B. Huang, Early diagnosis of urinary lithiasis via elementary profile of serum samples, Anal. Methods. 4 (2012) 693–698, https://doi.org/10.1039/c2ay05705k.
[42] X.-Y. Lou, R. Boada, V. Verdugo, L. Simonelli, G. Pérez, M. Valiente, Decoupling the adsorption mechanisms of arsenate at molecular level on modified cube-shaped sponge loaded superparamagnetic iron oxide nanoparticles, J. Environ. Sci. 121 (2022) 1–12, https://doi.org/10.1016/j.jes.2021.09.001.
[43] A. Politzer, J.C. H Teng, T.T. Singh, T.J.C. H, T.T. Singh, The method of producing a regenerated cellulose sponge, 1963. https://lens.org/073-184-824-742-697.
[44] P.E.L. Kyle, T.B. P, Ion exchange polymers on improved porous substrates, 1982. https://lens.org/080-517-023-858-186.
[45] X.Y. Lou, R. Boada, L. Simonelli, M. Valiente, Enhanced arsenite removal by superparamagnetic iron oxide nanoparticles in-situ synthesized on a commercial cube-shape sponge: adsorption-oxidation mechanism, J. Colloid Interface Sci. 614 (2022) 460–467, https://doi.org/10.1016/j.jcis.2022.01.119.
[46] N.B. Rainer, R.N. B, Polymer product for the selective absorption of dissolved ions, 1992. https://lens.org/018-286-240-697-194.
[47] J.A. Muñoz, A. Gonzalo, M. Valiente, J. O S E Ä A N T O N I O M U N˜ O Z, A N N A G O N Z A L O, A N D M A N U E L V A L I E N T E, J.A. Muñoz, A. Gonzalo, M. Valiente, Arsenic Adsorption by Fe(III)-Loaded Open-Celled Cellulose Sponge. Thermodynamic and Selectivity Aspects, Environ. Sci. Technol. 36 (2002) 3405–3411. https://doi.org/10.1021/es020017c.
[48] J. Li, L.P. Zhang, F. Peng, J. Bian, T.Q. Yuan, F. Xu, R.C. Sun, Microwave-assisted solvent-free acetylation of cellulose with acetic anhydride in the presence of iodine as a catalyst, Molecules 14 (2009) 3551–3566, https://doi.org/10.3390/molecules14093551.
[49] T. Burks, M. Avila, F. Akhtar, M. Göthelid, P.C. Lansåker, M.S. Toprak, M. Muhammed, A. Uheida, Studies on the adsorption of chromium(VI) onto 3-Mercaptopropionic acid coated superparamagnetic iron oxide nanoparticles, J. Colloid Interface Sci. 425 (2014) 36–43, https://doi.org/10.1016/j.jcis.2014.03.025.
[50] C. Han, K. Xu, Q. Liu, X. Liu, J. Li, Colorimetric sensing of cysteine using label-free silver nanoparticles, Sensors Actuators, B Chem. 202 (2014) 574–582, https://doi.org/10.1016/j.snb.2014.05.139.
[51] K.H. Glover, H. Tsubomura, Compounds with zinc (II), cadmium (II), mercury (II), J. Am. Chem. Soc. 87 (1965) 1904–1909.
[52] S. Aryal, B.K.C. Remant, N. Dharmaraj, N. Bhattarai, C.H. Kim, H.Y. Kim, Spectroscopic identification of SAu interaction in cysteine capped gold

nanoparticles, Spectrochim. Acta - Part A Mol. Biomol. Spectrosc. 63 (2006) 160–163, https://doi.org/10.1016/j.saa.2005.04.048.
[53] A. Ihs, B. Liedberg, Chemisorption of l-cysteine and 3-mercaptopropionic acid on gold and copper surfaces: an infrared reflection-absorption study, J. Colloid Interface Sci. 144 (1991) 282–292, https://doi.org/10.1016/0021-9797(91)90259-B.
[54] R. Alimohammadzadeh, A.A. Rafi, L. Goclik, C.W. Tai, A. Cordova, Direct organocatalytic thioglycolic acid esterification of cellulose nanocrystals: a simple entry to click chemistry on the surface of nanocellulose, Carbohydr. Polym. Technol. Appl. 3 (2022), 100205, https://doi.org/10.1016/j.carpta.2022.100205.
[55] H.Y. Choi, J.H. Bae, Y. Hasegawa, S. An, I.S. Kim, H. Lee, M. Kim, Thiol-functionalized cellulose nanofiber membranes for the effective adsorption of heavy metal ions in water, Carbohydr. Polym. 234 (2020), 115881, https://doi.org/10.1016/j.carbpol.2020.115881.
[56] K. Pramanik, P. Sarkar, D. Bhattacharyay, 3-Mercapto-propanoic acid modified cellulose filter paper for quick removal of arsenate from drinking water, Int. J. Biol. Macromol. 122 (2019) 185–194, https://doi.org/10.1016/j.ijbiomac.2018.10.065.
[57] G.H. Gao, M.J. Park, Y. Li, G.H. Im, J.H. Kim, H.N. Kim, J.W. Lee, P. Jeon, O. Y. Bang, J.H. Lee, D.S. Lee, The use of pH-sensitive positively charged polymeric micelles for protein delivery, Biomaterials 33 (2012) 9157–9164, https://doi.org/10.1016/j.biomaterials.2012.09.016.
[58] M. Pavelka, M.F.A. Lucas, N. Russo, On the hydrolysis mechanism of the second-generation anticancer drug carboplatin, Chem. - A Eur. J. 13 (2007) 10108–10116, https://doi.org/10.1002/chem.200700887.
[59] M. Sooriyaarachchi, A. Narendran, J. Gailer, Comparative hydrolysis and plasma protein binding of cis-platin and carboplatin in human plasma in vitro, Metallomics 3 (2011) 49–55, https://doi.org/10.1039/c0mt00058b.
[60] X.L. Yang, A.H.J. Wang, Structural studies of atom-specific anticancer drugs acting on, DNA (1999), https://doi.org/10.1016/S0163-7258(99)00020-0.
[61] W.J.F. van der Vijgh, Clinical pharmacokinetics of carboplatin, Clin. Pharmacokinet. 21 (1991) 242–261, https://doi.org/10.2165/00003088-199121040-00002.
[62] A.J. Di Pasqua, J. Goodisman, J.C. Dabrowiak, Understanding how the platinum anticancer drug carboplatin works: from the bottle to the cell, Inorganica Chim. Acta. 389 (2012) 29–35, https://doi.org/10.1016/j.ica.2012.01.028.
[63] J. Wang, J. Tao, S. Jia, M. Wang, H. Jiang, Z. Du, The protein-binding behavior of platinum anticancer drugs in blood revealed by mass spectrometry, Pharmaceuticals. 14 (2021) 1–17, https://doi.org/10.3390/ph14020104.
[64] D. Wang, S.J. Lippard, Cellular processing of platinum anticancer drugs, Nat. Rev. Drug Discov. 4 (2005) 307–320, https://doi.org/10.1038/nrd1691.
[65] K.U. Maheswari, T. Ramachandran, D. Rajaji, Interaction of cisplatin with planar model membranes - dose dependent change in electrical characteristics, Biochim. Biophys. Acta - Biomembr. 1463 (2000) 230–240, https://doi.org/10.1016/S0005-2736(99)00189-3.
[66] G. Speelmans, W.H.H.M. Sips, R.J.H. Grisel, R.W.H.M. Staffhorst, A.M. J. Fichtinger-Schepman, J. Reedijk, B. De Kruijff, The interaction of the anti-cancer drug cisplatin with phospholipids is specific for negatively charged phospholipids and takes place at low chloride ion concentration, Biochim. Biophys. Acta - Biomembr. 1283 (1996) 60–66, https://doi.org/10.1016/0005-2736(96)00080-6.
[67] T. Zimmermann, F. Šebesta, J.V. Burda, A new grand-canonical potential for the thermodynamic description of the reactions in solutions with constant pH, J. Mol. Liq. 335 (2021) 115979.
[68] J.R. Yachnin, I. Wallin, R. Lewensohn, F. Sirzén, H. Ehrsson, The kinetics and cytotoxicity of cisplatin and its monohydrated complex, Cancer Lett. 132 (1998) 175–180, https://doi.org/10.1016/S0304-3835(98)00175-X.
[69] E. Curis, K. Provost, D. Bouvet, I. Nicolis, S. De Crauste-Manciet, D. De Brossard, S. Bénazeth, Carboplatin and oxaliplatin decomposition in chloride medium, monitored by XAS, J. Synchrotron Radiat. 8 (2001) 716–718, https://doi.org/10.1107/S0909049500017775.
[70] G. Feiqiang, L. Xiaolei, J. Xiaochen, Z. Xingmin, G. Chenglong, R. Zhonghao, Characteristics and toxic dye adsorption of magnetic activated carbon prepared from biomass waste by modified one-step synthesis, Colloids Surfaces A Physicochem. Eng. Asp. 555 (2018) 43–54, https://doi.org/10.1016/j.colsurfa.2018.06.061.
[71] S. Sen Gupta, K.G. Bhattacharyya, Kinetics of adsorption of metal ions on inorganic materials: a review, Adv. Colloid Interface Sci. 162 (2011) 39–58, https://doi.org/10.1016/j.cis.2010.12.004.
[72] J. Wang, X. Guo, Adsorption kinetic models: physical meanings, applications, and solving methods, J. Hazard. Mater. 390 (2020), 122156, https://doi.org/10.1016/j.jhazmat.2020.122156.
[73] M. Mourabet, H. El Boujaady, A. El Rhilassi, H. Ramdane, M. Bennani-Ziatni, R. El Hamri, A. Taitai, Defluoridation of water using brushite: equilibrium, kinetic and thermodynamic studies, Desalination 278 (2011) 1–9, https://doi.org/10.1016/j.desal.2011.05.068.
[74] D. Han, X. Li, Z. Gong, L. Jiang, Z. Wang, P. Liu, Hierarchical porous catalytic pyrolysis char derived from oily sludge for enhanced adsorption, ACS Omega 6 (2021) 20549–20559, https://doi.org/10.1021/acsomega.1c02575.
[75] V.D. Chinh, L.X. Hung, L. Di Palma, V.T.H. Hanh, G. Vilardi, Effect of carbon nanotubes and carbon nanotubes/gold nanoparticles composite on the photocatalytic activity of TiO2 and TiO2-SiO2, Chem. Eng. Technol. 42 (2019) 308–315, https://doi.org/10.1002/ceat.201800265.
[76] G. Los, M.J.H. Van Vugt, L. Den Engelse, H.M. Pinedo, Effects of temperature on the interaction of cisplatin and carboplatin with cellular DNA, Biochem. Pharmacol. 46 (1993) 1229–1237, https://doi.org/10.1016/0006-2952(93)90472-9.
[77] M.A. Allsopp, G.J. Sewell, C.G. Rowland, C.M. Riley, R.L. Schowen, The degradation of carboplatin in aqueous solutions containing chloride or other selected nucleophiles, Int. J. Pharm. 69 (1991) 197–210, https://doi.org/10.1016/0378-5173(91)90362-R.
[78] J. Wang, X. Guo, Adsorption isotherm models: classification, physical meaning, application and solving method, Chemosphere 258 (2020), 127279, https://doi.org/10.1016/j.chemosphere.2020.127279.
[79] R.D. Hancock, A.E. Martell, Ligand design for selective complexation of metal ions in aqueous solution, Chem. Rev. 89 (1989) 1875–1914, https://doi.org/10.1021/cr00098a011.
[80] A. Alfarra, E. Frackowiak, F. Béguin, The HSAB concept as a means to interpret the adsorption of metal ions onto activated carbons, Appl. Surf. Sci. 228 (2004) 84–92, https://doi.org/10.1016/j.apsusc.2003.12.033.
[81] P. Pourhakkak, A. Taghizadeh, M. Taghizadeh, M. Ghaedi, S. Haghdoust, Fundamentals of adsorption technology, 1st ed., Elsevier Ltd., 2021. https://doi.org/10.1016/B978-0-12-818805-7.00001-1.
[82] M. Sun, Y. Yang, M. Huang, S. Fu, Y. Hao, S. Hu, D. Lai, L. Zhao, Adsorption behaviors and mechanisms of antibiotic norfloxacin on degradable and nondegradable microplastics, Sci. Total Environ. 807 (2022), 151042, https://doi.org/10.1016/j.scitotenv.2021.151042.
[83] R.M. Schneider, C.F. Cavalin, M.A.S.D. Barros, C.R.G. Tavares, Adsorption of chromium ions in activated carbon, Chem. Eng. J. 132 (2007) 355–362, https://doi.org/10.1016/j.cej.2007.01.031.
[84] S. Guo, M. Gao, T. Shen, Y. Xiang, G. Cao, Effective adsorption of sulfamethoxazole by novel organo-Vts and their mechanistic insights, Microporous Mesoporous Mater. 286 (2019) 36–44, https://doi.org/10.1016/j.micromeso.2019.05.032.
[85] Z. Gu, M. Gao, Z. Luo, L. Lu, Y. Ye, Y. Liu, Bis-pyridinium dibromides modified organo-bentonite for the removal of aniline from wastewater: a positive role of π-π Polar interaction, Appl. Surf. Sci. 290 (2014) 107–115, https://doi.org/10.1016/j.apsusc.2013.11.008.
[86] S.F. Soares, J. Nogueira, T. Trindade, A.L. Daniel-da-Silva, Towards efficient ciprofloxacin adsorption using magnetic hybrid nanoparticles prepared with κ-, ι-, and λ-carrageenan, J. Nanostructure Chem. 13 (2022) 283–302, https://doi.org/10.1007/s40097-022-00498-x.
[87] S. Kishani, T. Benselfelt, L. Wågberg, J. Wohlert, Entropy drives the adsorption of xyloglucan to cellulose surfaces – a molecular dynamics study, J. Colloid Interface Sci. 588 (2021) 485–493, https://doi.org/10.1016/j.jcis.2020.12.113.
[88] G.D. Değermenci, N. Değermenci, V. Ayvaoğlu, E. Durmaz, D. Çakır, E. Akan, Adsorption of reactive dyes on lignocellulosic waste; characterization, equilibrium, kinetic and thermodynamic studies, J. Clean. Prod. 225 (2019) 1220–1229, https://doi.org/10.1016/j.jclepro.2019.03.260.
[89] T. Yoshinaga, Y. Iso, T. Isobe, Optimizing the microwave-assisted hydrothermal synthesis of blue-emitting L-cysteine-derived carbon dots, J. Lumin. 213 (2019) 6–14, https://doi.org/10.1016/j.jlumin.2019.05.003.
[90] V. Sharma, P. Ilaiyaraja, A.C. Dakshinamurthy, C. Sudakar, One step thermolysis of Sb-Mercaptopropionic acid complex in ambient air atmosphere for growing Sb2S3 thin films with controlled microstructure, Mater. Sci. Semicond. Process. 121 (2021), 105330, https://doi.org/10.1016/j.mssp.2020.105330.
[91] M. Mrad, T. Ben Chaabane, H. Rinnert, B. Lavinia, J. Jasniewski, G. Medjahdi, R. Schneider, Aqueous synthesis for highly emissive 3-mercaptopropionic acid-capped AIZS quantum dots, Inorg. Chem. 59 (2020) 6220–6231, https://doi.org/10.1021/acs.inorgchem.0c00347.
[92] W. Jian, S. Liu, J. Li, W. Yang, Decomposition reaction of Zn-MPA(3-mercaptopropionic acid) complex under microwave irradiation, Chem. Res. Chinese Univ. 24 (3) (2008) 353–356.
[93] R. Micanovic, K. Lafavers, P.S. Garimella, X.R. Wu, T.M. El-Achkar, Uromodulin (Tamm-Horsfall protein): guardian of urinary and systemic homeostasis, Nephrol. Dial. Transplant. 35 (2020) 33–43, https://doi.org/10.1093/ndt/gfy394.
[94] S. Aitekenov, A. Gaipov, R. Bukasov, Review: detection and quantification of proteins in human urine, Talanta 223 (2021), 121718, https://doi.org/10.1016/j.talanta.2020.121718.
[95] L. Curtis, A. Turner, N. Vyas, G. Sewell, Speciation and reactivity of cisplatin in river water and seawater, Environ. Sci. Technol. 44 (2010) 3345–3350, https://doi.org/10.1021/es903620z.